Robust Multi-Legged Walking Robots for Interactions with Different Terrains

Nina Robson
Mechanical Engineering
California State University Fullerton
Email: nrobson@fullerton.edu
Mechanical and Aerospace Engineering
University of California, Irvine
Email: npatarin@uci.edu

Vanessa Audrey *
Mechanical and Aerospace Engineering
University of California, Irvine
Email: vaudrey@uci.edu

Ashutosh Dwivedi
Mechanical Engineering
California State University Fullerton
Fullerton, California, 92834
ashutoshd@csu.fullerton.edu

Dylan Kunzmann
Mechanical Engineering
California State University Fullerton
Fullerton, California, 92834
dylankunzmann@csu.fullerton.edu

ABSTRACT

This paper explores the kinematic synthesis, design and pilot experimental testing of a six-legged walking robotic platform able to traverse through different terrains. We aim to develop a structured approach to designing the limb morphology using a relaxed kinematic task with incorporated conditions on foot-environments interaction, specifically contact force direction and curvature constraints, related to maintaining contact. The design approach builds up incrementally starting with studying the basic human leg walking trajectory and then defining a "relaxed" kinematic task. The "relaxed" kinematic task consists only of two contact locations (toe-off and heel-strike) with higher order motion task specifications compatible with foot-terrain(s) contact and curvature constraints in the vicinity of the two contacts. As the next step, an eight-bar leg image is created based on the "relaxed" kinematic task and incorporated within a six-legged walking robot. Pilot exper-

*Address all correspondence to this author.

imental tests explore if the proposed approach results in an adaptable behavior which allows the platform to incorporate different walking foot trajectories and gait styles coupled to each environment. The results suggest that the proposed "relaxed" higher order motion task combined with the leg morphological properties and feet material allowed the platform to walk stably on the different terrains.

Here we would like to note that one of the main advantages of the proposed method in comparison with other existing walking platforms is that the proposed robotic platform has carefully designed limb morphology with incorporated conditions on foot-environment interaction. Additionally, while most of the existing multi-legged platforms incorporate one actuator per leg, or per joint, our goal is to explore the possibility of using a single actuator to drive all six legs of the platform. This is a critical step which opens the door for the development of future transformative technology that is largely independent of human control and able to learn about the environment through their own sensory systems.

INTRODUCTION

Multi-legged robots [1] have many unique advantages over wheeled and tracked systems in terms of gaining access to and maintaining locomotion efficiency on rough and unstructured terrain. This makes them ideally suited for applications such as disaster response, remote inspection and exploration in many different environments. Within the field of legged robotics, multi-legged robots are understood as having four or more legs, in contrast to bipedal or humanoid robots. In recent years, bipedal or humanoid robots have been tested in environments designed for humans and using human tools and machinery and there is significant research going on in human-sized and shaped robots; however, their morphologies also impose substantial challenges in regard to dynamic control of bipedal walking, system stability, ability to recover from actuator failures, and others. In contrast, multi-legged robots designs are typically inspired by quadruped mammals and hexapedal or octopedal arthropods. These robots have significant advantages over bipedal systems in regard to dynamics, stability, and ability to negotiate challenging terrain. Most of the

existing multi-legged robot platforms for walking on unstructured terrains use either four or six legs, each of which is a four-bar linkage ([2], [3], [4], [5]), or planar and spatial serial chains ([6], [7], [8], [9]). While the RHex robot for example, [10], [11], incorporates six actuators for each of the six springy "compass" type legs for negotiating stairs and relatively badly broken stiff terrains at relatively high speeds, we aim at developing a structured approach to designing the limb morphology using a relaxed kinematic task with incorporated conditions on foot-environments normal direction and curvature constraints. Moreover, our goal is to explore the possibility of using a single actuator to drive all six legs and finally test if the proposed approach results in an adaptable behavior which allows the platform to incorporate different walking trajectories and gait styles coupled to each environment without explicit control.

Contemporary mechanism design relies upon constrained problem formulation by specifying the kinematic task for the motion to be achieved, a set of alternative mechanisms to be used, and typically considers the mechanisms and the objects or the environment as rigid. This had led to the design of single-purpose mechanisms. One of the main challenges of using legged robots in practical applications is how to control and adapt their gait to different terrains, that is finding a suitable and adaptable foot displacement trajectory, similar to the way that humans or animals walk adaptively and effectively under a variety of speeds and terrains [12]. The literature shows a variety of design strategies to generate gait patterns, including adaptive locomotion control [13], use of hybrid locomotive mechanisms [14], combination of rigid and tensile structural elements [15], joint torque and position control of compliant legs [16], morphological computation [17], oscillator controller with pneumatic actuators [18], and biomimetic adaptations based on ground contact timing [19], or using sensorimotor coordination [20]. A reconfigurable design approach is presented in [21], where a robot can vary its hardware morphology by parametric changes of its components. In particular, the paper reports a novel reconfigurable Theo Jansen linkage that produces a variety of gait cycles. The standard Theo Jansen linkage [22] is a popular closed kinematic chain suitable for developing legged robots. Such pin-jointed planar linkage operates with only one actuator. The proposed design in [21] extends the capabilities of the original mechanism, while maintaining its mechanical simplicity during normal operation, generating different gait patterns. The authors

outline main challenges in designing a reconfigurable version of a Theo Jansen linkage, such as the development of efficient approaches to trace foot trajectories, that is, coupler curves, the definition of the novelty and utility of the resulting foot trajectories, the development of heuristics to guide the reconfiguration process, and the non-trivial process of implementing theoretical designs generated analytically into physical mechanisms.

In this paper we take a different approach, through exploring if a specification of a foot-environment contact kinematic task, combined with carefully designed leg morphology and choice of foot material will result in an adaptable behavior which allows the platform to incorporate different walking foot trajectories and gait styles coupled to each environment. Our design process starts with the specification of the ”relaxed” walking kinematic task consisting of only two contact locations (toe-off and heel-strike) with higher order kinematic specifications, compatible with foot-environments contact and curvature constraints. As a next step, we create a walking robot with six legs, each of which is an eight-bar kinematic chain, which design is based on the ”relaxed” higher order motion task. Finally, we experimentally test the ability of the robot platform to traverse through different terrains, such as pavement, sand, and grass.

BACKGROUND: UNDERSTANDING CONTACT DIRECTION AND CURVATURE CONSTRAINTS IN THE VICINITY OF A BODY-ENVIRONMENT CONTACT LOCATION

Let the movement of a rigid body AB be defined by the 3×3 homogeneous transform $[T(t)] = [R(t), \mathbf{d}(t)]$ constructed from a rotation matrix, $R(t)$, and translation vector $\mathbf{d}(t)$. In the particular example of a foot contacting the ground in Figure 1, $\mathbf{A}$ and $\mathbf{B}$ represent the locations of the heel and the toe. Any point $\mathbf{p}$ on the foot with an attached moving frame M traces a trajectory $\mathbf{P}(t)$ in a fixed coordinate frame F, given by

$$\mathbf{P}(\mathbf{t}) = [T(t)]\mathbf{p} = \begin{bmatrix} \cos\phi(t) & -\sin\phi(t) & d_x(t) \\ \sin\phi(t) & \cos\phi(t) & d_y(t) \\ 0 & 0 & 1 \end{bmatrix} \begin{Bmatrix} p_x \\ p_y \\ 1 \end{Bmatrix} \tag{1}$$

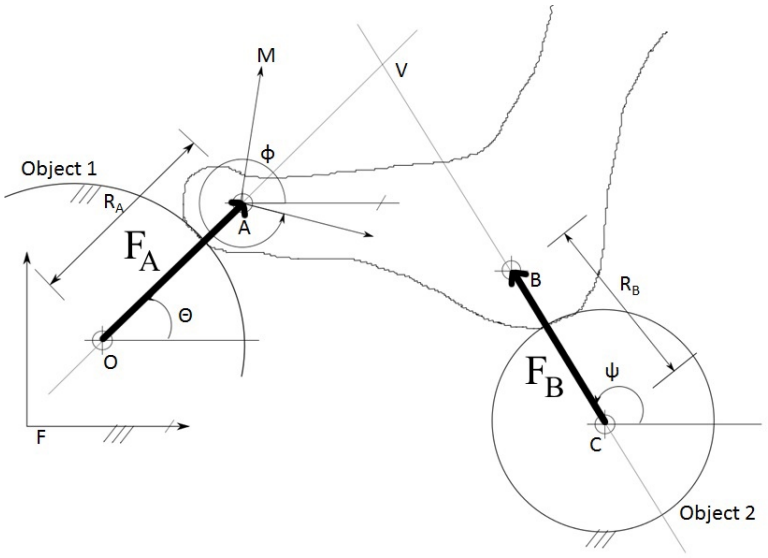

Fig. 1. A body with attached frame M moves in the vicinity of specified location and is in contact with two objects such that the trajectories of $\mathbf{A}$ and $\mathbf{B}$ have the radii of curvature, R_A and R_B, respectively. Note that the geometry setup is related to one contact location (either toe-off or heel-strike).

Higher Order Kinematic Specifications Compatible with Body-Environment Contact and Curvature

Assuming that the foot AB moves in contact with two fixed objects in the environment constrain the point trajectories $\mathbf{A}(t)$ and $\mathbf{B}(t)$ to move on circles in the vicinity of a reference position denoted by $t = 0$ (see Figure 1). The movement of the body in the vicinity of $t = 0$ can be expressed as the Taylor series expansion,

$$[T(t)] = [T_0] + [T_1]t + \frac{1}{2}[T_2]t^2 + ..., \quad \text{where} \quad [T_i] = \frac{d^i[T]}{dt^i} \tag{2}$$

and $[T_0]$ can be specified using the data provided for the position of the moving frame M that identifies the coordinates of the contact points $\mathbf{A_0} = \mathbf{A}(0)$ and $\mathbf{B_0} = \mathbf{B}(0)$.

The directions of the velocities vectors $\dot{\mathbf{A}}$ and $\dot{\mathbf{B}}$ are set to be perpendicular to the forces $\mathbf{F_A}$ and $\mathbf{F_B}$ by defining the point of intersection $\mathbf{V}$ of the lines of actions of these two forces to be the velocity pole of the movement of M in this position (Figure 1). This allows the calculation of the angular velocities $\mathbf{w_{OA}} = \dot{\theta}\vec{k}$ and $\mathbf{w_{CB}} = \dot{\psi}\vec{k}$. The velocity loop equations of the quadrilateral $\mathbf{OABC}$ are then used to compute the velocity $\dot{\mathbf{B}} = \dot{\mathbf{A}} + \mathbf{w} \times (\mathbf{B} - \mathbf{A})$. The angular velocity $\phi_1 = \dot{\phi}(0)$ and the velocity $\mathbf{d_1} = \dot{\mathbf{A}}(0)$ define the elements of the velocity matrix $[T_1]$.

As the body M moves in contact with two objects, the points A and B are guided along trajectories with radii of curvature R_A and R_B. The acceleration loop equations of the quadrilateral $\mathbf{OABC}$ can be used to determine the angular accelerations $\mathbf{a_{OA}} = \ddot{\theta}\vec{k}$ and $\mathbf{a_{CB}} = \ddot{\psi}\vec{k}$ for a given value of the angular acceleration $\mathbf{a} = \ddot{\phi}\vec{k}$. This in turn allows the derivation of $\ddot{\mathbf{d}} = \ddot{\mathbf{A}}$. The acceleration loop equations are obtained by computing the time derivative of the velocity loop equations. The values $\phi_2 = 0$ and $\mathbf{d_2} = \ddot{\mathbf{A}}(0)$ determine the elements of the acceleration matrix $[T_2]$. For more details on deriving the higher order motion task specification related to contact and curvature constraints, see [23], [24].

Apart from deriving the higher order motion constraints from the body-environment contact task geometry, as explained above, they can also be determined experimentally, by using Motion Capture system. In what follows we explore the incorporation of velocities and accelerations in the vicinity of two foot-environments contact locations within the kinematic task for the design of an eight-bar linkage robotic leg to be further used in the creation of a multi-legged walking robotic platform.

DESIGN OF AN EIGHT-BAR LEG MECHANISM BASED ON "RELAXED" KINEMATIC TASK

The general design procedure for the rover leg follows recent works of Robson et al. [25], [26], [27], [28]. It consists of the following stages: physiological contact task specification with higher order motion constraints, linkage topology selection, dimensional synthesis, and design evaluation. To facilitate the design process, a human subject walking on a treadmill was monitored by 3D Motion Capture System. Eight reflective markers were attached on the subjects right leg and the trajectories at the foot and knee joints were obtained. Figure 2 presents the knee gait trajectory for one cycle, as well as the target foot trajectory relative to the fixed thigh frame. Note that the geometrical shape of the reference foot trajectory looks like a teardrop for each gait cycle. Data for the additional trajectories from walking on sand is adopted from [29].

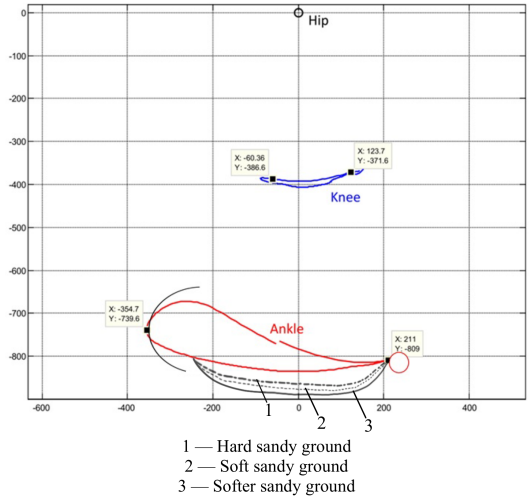

Fig. 2. Natural walking gait cycle trajectories at foot and knee level, obtained from the Motion Capture System. Data for the additional three foot trajectories observable from walking on sand are adopted from [29] and incorporated to the "flat" teardrop foot trajectory.

The Task Specification

After identifying the desired walking motion, we mathematically describe it as a physiological kinematic task. Sagittal plane walking motion can be assumed as a planar task which consists of positioning the foot, at the point, $Mj(j = 1, \ldots, n)$, located on the reference trajectory. To obtain a design with a potential for an adaptable foot displacement trajectory, instead of utilizing all points on the trajectory, we "relax" the task, by specifying only two foot-environment contact

locations (heel-strike and toe-off) each of which incorporates one velocity, compatible with the foot-environment contact forces. Note that the velocity specified at the toe off location was averaged, based on the four different curvatures (treadmill, hard sand, soft sand, and softer sand). An acceleration constraint is also specified in the vicinity of the heel strike contact location, where curvature constraints related to local motion properties, as well as desired shape and height of the walking trajectory are important for the overall performance of the mechanical leg. The velocities and acceleration are derived from the task geometry and it is expected that they are expressive enough to describe the leg's desired behavior in the vicinity of the two contacts, while still allowing flexibility in the foot trajectory between those contacts. The eight-bar leg design starts with scaling down the "relaxed" foot motion task at knee level, and synthesizing a four-bar linkage, based on the scaled down "relaxed" task [30].

The Synthesis Equations

To design the four bar linkage at knee level, we first formulate the design equations of a planar RR chain for the "relaxed" scaled down task, consisting of two contact locations with velocity and acceleration specifications, listed in Table 1.

Table 1. Task data for the synthesis of a planar RR chain based on the "relaxed" scaled down motion task

Posit.	(ϕ, d_x, d_y)	Vel. Data	Accel. Data
1	(0, 2.2, 1.44)	(1, 0.33, 0.93)	(0, 0.29, 0.81)
2	(0, 3.2, 1.25)	(1, -0.03, -0.83)	—

The planar RR chain has five design parameters the coordinates of the fixed pivot $\mathbf{G} = (u, v, 1)$ in the fixed frame F, the coordinates of the moving pivot $\mathbf{w}$ in the moving frame M, and the length of the crank R. The geometry of the RR chain satisfies the constraint equation:

$$(\mathbf{W} - \mathbf{G}) \cdot (\mathbf{W} - \mathbf{G}) = R^2, \tag{3}$$

where $\mathbf{W}$ defines the fixed frame coordinates of the moving pivot $\mathbf{w}$ as $\mathbf{W}(t) = [T(t)]\mathbf{w}$. The

first two time derivatives of this equation yield the additional velocity and acceleration constraint equations

$$\begin{aligned} \dot{\mathbf{W}} \cdot (\mathbf{W} - \mathbf{G}) =& 0, \\ \ddot{\mathbf{W}} \cdot (\mathbf{W} - \mathbf{G}) + \dot{\mathbf{W}} \cdot \dot{\mathbf{W}} =& 0. \end{aligned} \tag{4}$$

The Design Equations

Let $\mathbf{W^1} = (x, y, 1)$, so we have

$$\begin{aligned} \mathbf{W^1}(\mathbf{t}) = [D^1(t)]\mathbf{W^1} =& [I + \Omega^1 t + \frac{1}{2}\Lambda^1 t^2]\mathbf{W^1}, \\ \mathbf{W^2}(\mathbf{t}) = [D^2(t)]\mathbf{W^2} =& [I + \Omega^2 t][D_{12}]\mathbf{W^1}, \end{aligned} \tag{5}$$

where $[D_{12}] = [{T_0}^2][{T_0}^1]^{-1}$ yields $\mathbf{W^2} = [D_{12}]\mathbf{W^1}$.

We substitute the trajectories (5) into the constraint equations (3) and (4) to obtain the design equations for the RR chain, shown in (6).

$$\begin{aligned} \mathcal{P}_1 : \quad & 0 = (\mathbf{W^1} - \mathbf{G}) \cdot (\mathbf{W^1} - \mathbf{G}) - R^2, \\ \mathcal{V}_1 : \quad & 0 = [\Omega^1]\mathbf{W^1} \cdot (\mathbf{W^1} - \mathbf{G}), \\ \mathcal{A}_1 : \quad & 0 = [\Lambda^1]\mathbf{W^1} \cdot (\mathbf{W^1} - \mathbf{G}) + [\Omega^1]\mathbf{W^1} \cdot [\Omega^1]\mathbf{W^1}, \\ \mathcal{P}_2 : \quad & 0 = ([D_{12}]\mathbf{W^1} - \mathbf{G}) \cdot ([D_{12}]\mathbf{W^1} - \mathbf{G}) - R^2, \\ \mathcal{V}_2 : \quad & 0 = [\Omega^2][D_{12}]\mathbf{W}^1 \cdot ([D_{12}]\mathbf{W^1} - \mathbf{G}). \end{aligned} \tag{6}$$

A detailed algebraic solution procedure of the synthesis incorporating tasks with acceleration specifications could be found in [23]. The four-bar was obtained by combining two real RR solutions,

resulting in a linkage with a very compact coupler, shown in Figure 3.

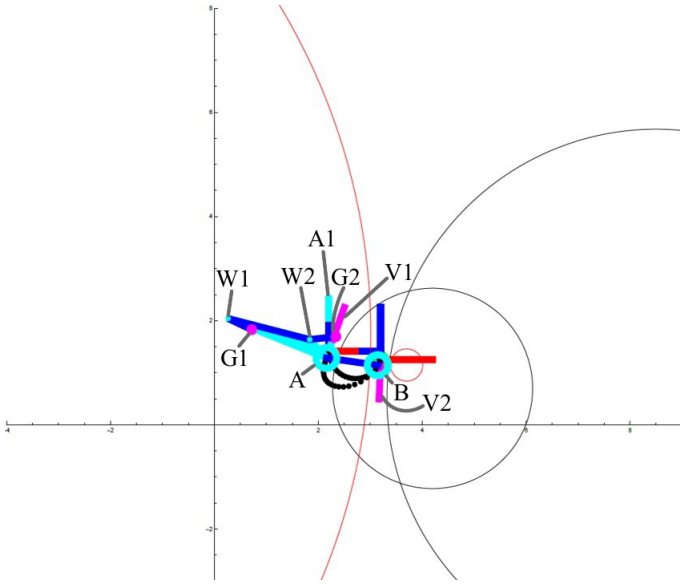

Fig. 3. The obtained four-bar linkage with a coupler trajectory based on the scaled down "relaxed" kinematic task consisting of two contact locations with higher order motion constraints.The base pivots are denoted by G1 and G2, while the moving pivots are W1 and W2. The coupler points **A** and **B** were already presented in Figure 1. Note that for this specific scaled down task, points **A** and **B** are at the knee level.

Trajectory Planning

The inverse kinematics of the 4R chain yields the joint parameter vector $\mathbf{q}$ at each of the task positions, $i = 1, 2$. In order to obtain the joint velocity vector $\dot{\mathbf{q}}$ at the ith position, we solve the equation

$$V_i = [J_i]\dot{\mathbf{q}}_\mathbf{i}, \quad i = 1, 2, \tag{7}$$

where $V_i = (\omega, \mathbf{v})$ is the velocity prescribed at position i, and J_i is the Jacobian of the 4R chain, resulting in:

$$\dot{\mathbf{q}}_{\mathbf{i}i} = [{J_i}^T J_i]^{-1}[{J_i}^T]V_i, \quad i = 1, 2. \tag{8}$$

Now to determine the joint acceleration vector $\ddot{\mathbf{q}}$, we solve the equation

$$A_i = \dot{J}_i\dot{\mathbf{q}}_i + J_i\ddot{\mathbf{q}}_i, \quad i = 1, \tag{9}$$

where $A_i = (\alpha, \mathbf{a})$ is the acceleration prescribed at the first position and $\dot{J}_i$ is the time derivative of the 3×2 Jacobian matrix. The vector $\dot{J}_i\dot{\mathbf{q}}_i$ is known so we can subtract it from both sides, thus the solution is again obtained using the pseudo-inverse,

$$\ddot{\mathbf{q}}_{\mathbf{i}} = [{J_i}^T J_i]^{-1}[{J_i}^T](A_i - \dot{J}_i\dot{\mathbf{q}}_i). \tag{10}$$

The trajectory between the joint parameters $(\theta_0, \dot{\theta_0}, \ddot{\theta_0})$ and $(\theta_f, \dot{\theta_f}, \ddot{\theta_f})$ over the range $0 \leq t \leq t_f$ is generated by the fifth degree polynomial

$$\theta(t) = a_0 + a_1t + a_2t^2 + a_3t^3 + a_4t^4 + a_5t^5, \tag{11}$$

where

$$
\begin{aligned}
a_0 =& \theta_0, \quad a_1 = \dot{\theta}_0, \quad a_2 = \frac{\ddot{\theta}_0}{2}, \\
a_3 =& \frac{20\theta_f - 20\theta_0 - (8\dot{\theta}_f + 12\dot{\theta}_0)t_f - (3\ddot{\theta}_0 - \ddot{\theta}_f)t_f^2}{2t_f^3}, \\
a_4 =& \frac{30\theta_0 - 30\theta_f + (14\dot{\theta}_f + 16\dot{\theta}_0)t_f + (3\ddot{\theta}_0 - 2\ddot{\theta}_f)t_f^2}{2t_f^4}, \\
a_5 =& \frac{12\theta_f - 12\theta_0 - (6\dot{\theta}_f + 6\dot{\theta}_0)t_f - (\ddot{\theta}_0 - \ddot{\theta}_f)t_f^2}{2t_f^5}.
\end{aligned} \tag{12}
$$

Equation (11) is obtained by solving the equations defining the joint position, velocity and acceleration evaluated at $t = 0$ and $t = t_f$ to compute the coefficients $a_i, i = 0, \ldots, 5$, see [31]. Figure 3 illustrates the movement of the coupler of the four bar linkage based on the knee-level "relaxed" task, shown in Table 1.

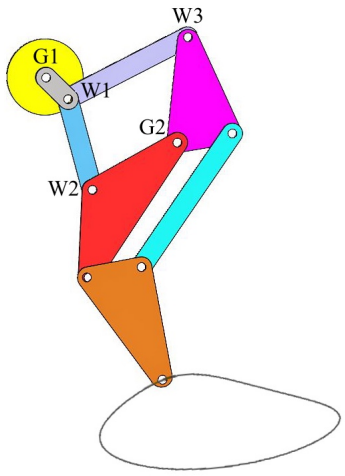

Fig. 4. The created eight-bar leg linkage with the resulting foot trajectory, based on the "relaxed" kinematic task. The eight-bar leg incorporates two four-bar linkages: the synthesized $G1G2W1W2$, as well as $G1G2W1W3$ that share the base frame and the driving link. A pantograph mechanism completes the design of the eight-bar leg by relocating and scaling up the resulting trajectory.

As a next step, a second four-bar linkage $G1G2W1W3$ that shares the base frame and the driving link with the synthesized one $G1G2W1W2$ is incorporated within the design and is shown in Figure

3. A pantograph mechanism relocates and scales up the foot trajectory [32], resulting in the eight-bar linkage shown in Figure 4. The link lengths of the resulting eight-bar linkage are given in Figure 5 and Table 2.

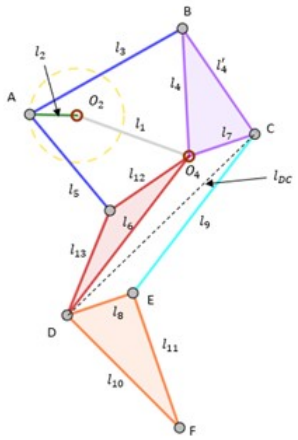

Fig. 5. Link lengths of the leg mechanism.

Fig. 6. CAD drawing of the rover platform that incorporates six legs, each of which is an eight-bar linkage.

PILOT TESTING OF THE WALKING ROVER PLATFORM

For the overall walking platform gait, the leg coordination of quadruped mammals and hexapedal arthropods was studied [33]. To reduce the cost and simplify the actuation of the preliminary prototype, all leg input cranks were connected through a gear train mechanism, so that the rover was driven by a single DC motor resulting in a periodic gait, which repeats with every rotation of

Table 2. Link lengths of the resulting eight-bar linkage

Linkage (l_x)	Link Length $(units)$
l_1	36
l_2	13
l_3	46
l_4 & l'_4	36
l_5	32
l_6	55
l_7	19
l_8	19
l_9	55
l_{10}	43
l_{11}	39
l_{12}	26
l_{13}	26

the input crank. The DC motor is powered by a 12-volt battery and controlled using a PWM speed controller. Three legs at a time were coordinated to form a tripod gait with a duty factor (fraction of time the leg touches the ground) of $\frac{1}{2}$. This is expected to yield a stable walking gait, since the tripod support pattern formed by the contact points of diagonally opposite legs includes the center of gravity of the walker. The CAD drawing of the walking rover platform is shown in Figure 6. The body was designed with Polylactic Acid material. To support the body of the walker, the feet were specifically created to provide an expanded contact surface area. To independently solve for the two forces F_A and F_B shown in Figure 1, two equations need to be defined, which requires the definition of two points in the moving body in the vicinity of a contact location (i.e. defining one point is not sufficient). By scaling up the results in Figure 3 the foot capsize has been determined and a flexible ball manufactured out of rubbery thermoplastic polyurethane (TPU) with a proper size has been used in the feet of the platform to ensure multiple contact points within a contact location and to increase the contact area within a contact location and traction for self-stabilization while traversing the different environments (see Figure 7).

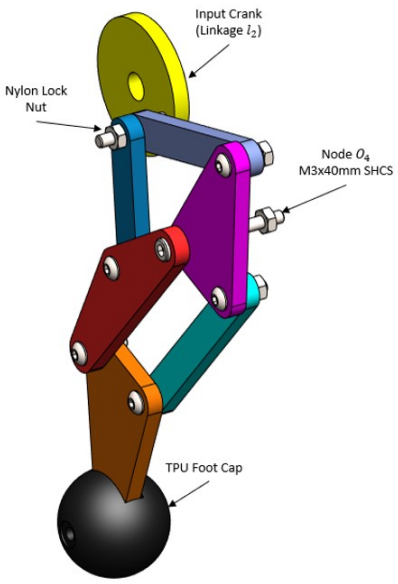

Fig. 7. In order to maximize surface area when traversing on deformable surfaces such as sand or grass, a spherical foot cap was designed. The foot cap size is based on the results in Figure 3. By scaling up results related to the locations of point A and B in Figure 3, the foot cap size/geometry has been determined.

The 3D printed preliminary rover prototype and the first series of experimental testing of its resulting foot trajectory while suspended in the air are shown in Figure 8. A GoPro camera shown in Figure 9 is continuously recording footage while the rover is in motion. Using Adobe After Effects (AAE), the camera footage is edited to incorporate an overlapped tracer module. The AAE tracer module uses X-Y position data from a desired pixel array set by the editor using the ”Track Motion” command. In the case of the leg mechanism, the tracer module was located near the TPU foot cap. Once the desired pixel array was set, a circle-shaped point was created to follow the tracer module data. The result is a path generated from the circle-shaped points and tracer data to model the rover's walking trajectory. As shown in the Figure 8, the resulting unloaded trajectory follows in general the shape of the desired trajectory from Figure 4.

Due to the lack of hard, soft, and softer sand terrains, Figure 10 presents the pilot testing of the preliminary prototype on sand (top), pavement (middle), and grass (bottom). The rover was tested under two conditions: traversing at 50% of the maximum velocity, which correlates to approximately 43 mm/s. This velocity was determined using real-time video footage of the rover's displacement over a known distance. Using the time stamp data from the recording in conjunction with the

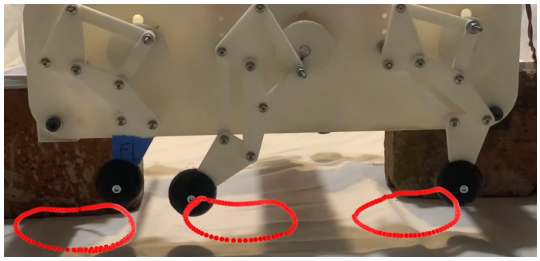

Fig. 8. 3D printed prototype of the walking rover and the resulting leg trajectory, while the platform is suspended in the air.

rover's position, the velocity was determined. The second condition was at maximum velocity, approximately 85 mm/s. As seen in the figures, different foot trajectories are observed when testing at the two different velocities.

Part of the stability of locomotion is attributed to the mechanical properties and part to the movement pattern of the system. To ensure the walker balance, the crank rotations of each leg were coordinated so there are always 3 feet in contact with the ground to support the body resulting in a tripod gate. The walking platform remains statically stable because its center of mass projects vertically inside the edges of the support triangle formed by the contact points. The authors refer to stability as the ability of the platform to maintain the movement pattern that it was initially designed for, i.e., the tripod gate with a duty factor of $\frac{1}{2}$ as a function of the stability margin for platforms with 6 legs [34]. The stability margin is defined as the minimum distance from the center of gravity projection to the edges of the support triangle. Initially, the ability of maintaining balance due to perturbations caused by objects in the environments at two different speeds was tested and a preferred speed was assigned to each terrain, based on the duty factor. As a next step, the ability of the rover to recover from perturbations (such as slip or trip) caused by the unstructured environments or from small slopes/holes in the environments at the preferred velocity was also tested.

Figure 11, Figure 12, and Figure 13 depict the gait pattern, i.e. time intervals that the Front-Right (FR), Middle-Right (MR), and Rear-Right (RR) legs are in contact with the surface. Note, that only the gait pattern on one side of the platform is shown, since the motion of the six legs of the platform are synchronized in a tripod gait. In general, with an increased speed, it is expected that the gait of the leg mechanism will produce shorter cycles since the foot spends less time in contact with the

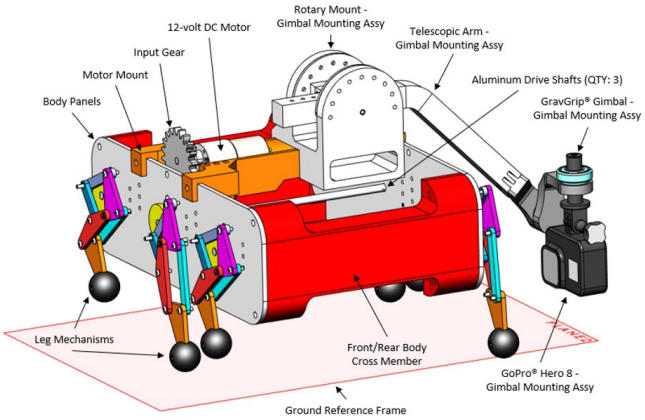

Fig. 9. Rover Design Breakdown (Front Isometric View).

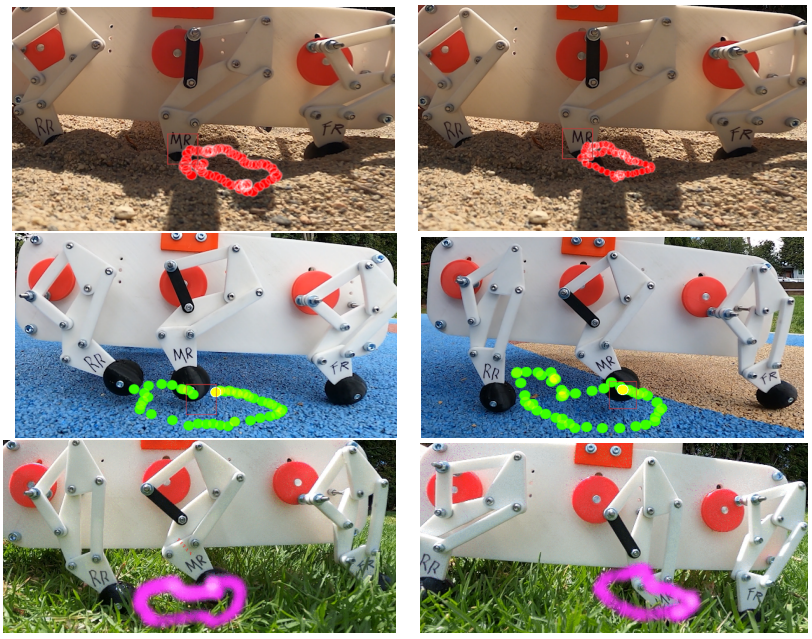

Fig. 10. Pilot testing of the preliminary prototype traversing sand (top), pavement (middle), and grass (bottom) terrains with two different velocities: 43 mm/s (left) and 85 mm/s (right). The walking trajectories are based on tracking the middle point of the middle foot of the rover platform.

ground. The tests on pavement and grass at higher speed resulted in a shorter foot-environment contact in comparison with the lower speed. As shown in Figure 12, the trajectory data at 43 mm/s reflects very different gaits. At 43 mm/s, the sand introduced a shorter returning path time. Different trajectories and gait patterns were also observed when testing at 85mm/s. The sand terrain revealed the longest contact interval whereas the pavement was the shortest at an average

of 0.6 seconds. With the porosity of the sand surface, the foot became further submerged as it was traversing, thus leading to an increase in surface contact time throughout the stride intervals and resulting in a $\frac{2}{3}$ duty factor. Note that due to the nature of some terrains, or the change of speed, when the duty factor increases ($\frac{2}{3}$, $\frac{3}{4}$, or 1 for example), the stability is improved [34].

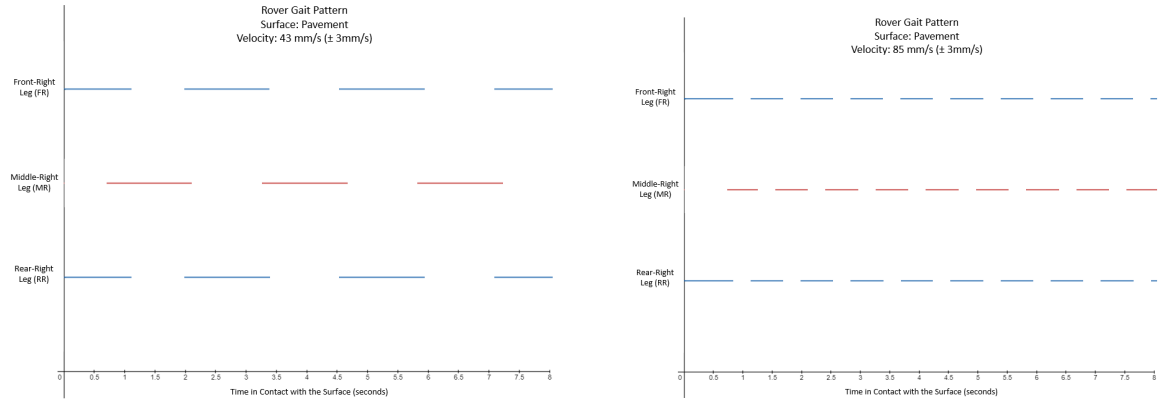

Fig. 11. Pavement gait patterns with velocities of 43 mm/s and 85 mm/s respectively. Note that due to the synchronized foot motion on both sides of the rover, only the gait pattern on the right-hand side is shown.

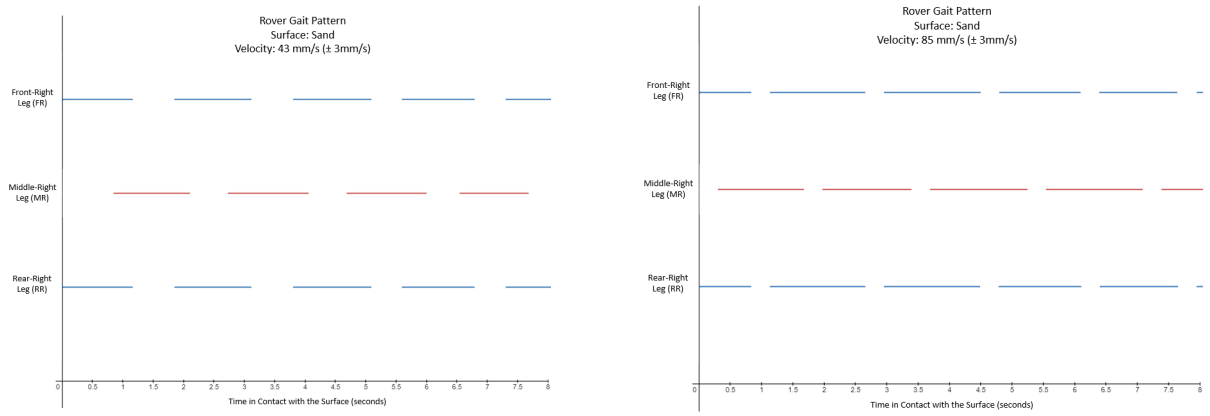

Fig. 12. Sand gait patterns with velocities of 43 mm/s and 85 mm/s respectively. Note that due to the synchronized foot motion on both sides of the rover, only the gait pattern on the right-hand side is shown.

With the trajectory and gait pattern data collected, an overlapped representation of the walking trajectories at 43 mm/s and 85 mm/s on each terrain is shown in Figure 14. The ”flat” walking trajectory from Figure 2 and the desired ”unstructured terrain” trajectory from Figure 4 are added

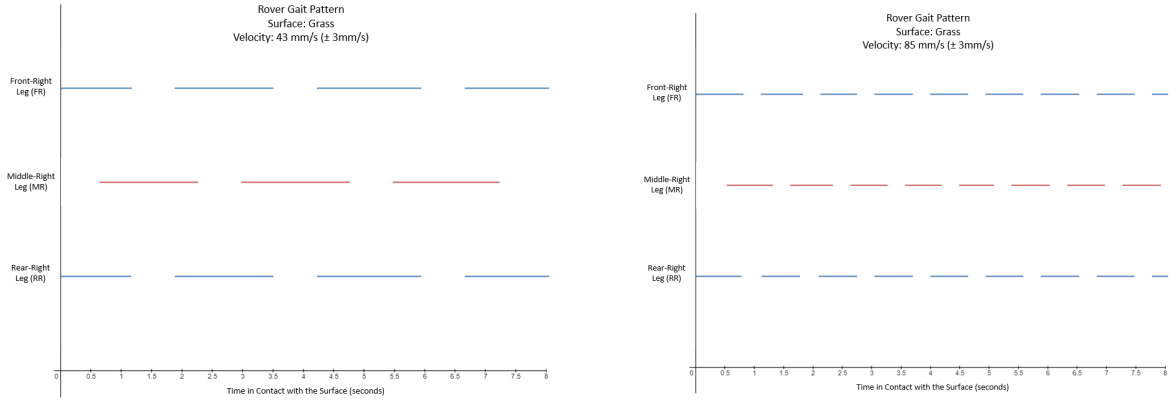

Fig. 13. Grass gait patterns with velocities of 43 mm/s and 85 mm/s respectively. Note that due to the synchronized foot motion on both sides of the rover, only the gait pattern on the right-hand side is shown.

for comparison. The X- and Y-axis represent the approximated dimension of the trajectories length and height. Overall, the pilot test results show that the rover is able to adapt to and stably traverse through the three terrains incorporating different walking foot trajectories and gait styles coupled to each environment without explicit control. Some of the shortcomings of the proposed design are that overcoming slopes have not been considered within the design of the initial platform. So far it has been assumed that the three feet contacts with the ground that support the body are co-planar and the walking system's center of mass projects vertically inside the support triangle of the contact points (for static stability). It is clear that if the contacts are made on tilted surfaces the "projection of the center of mass" criterion cannot discriminate correctly cases where the system can remain static from cases where it can't. Pilot testing of generalization of the platform performance to other environments shows that the final prototype can overcome up to 15 degrees slopes.

Recently, the walking platform has been further expanded to an increased scale final prototype. The rover chassis is constructed of aluminum extruded tubing with a space-frame design configuration. The legs are made from aluminum plate and mated to hollowed rubber feet. The drivetrain is optimized by incorporating a chain-driven pulley system coupled with bearing-loaded input cranks. The current testing of the final prototype on different terrains is shown in Figure 15. A video demonstration of the rover final prototype performance in the different environments can be seen in the following link: https://youtu.be/8Gn8gKT5kXo.

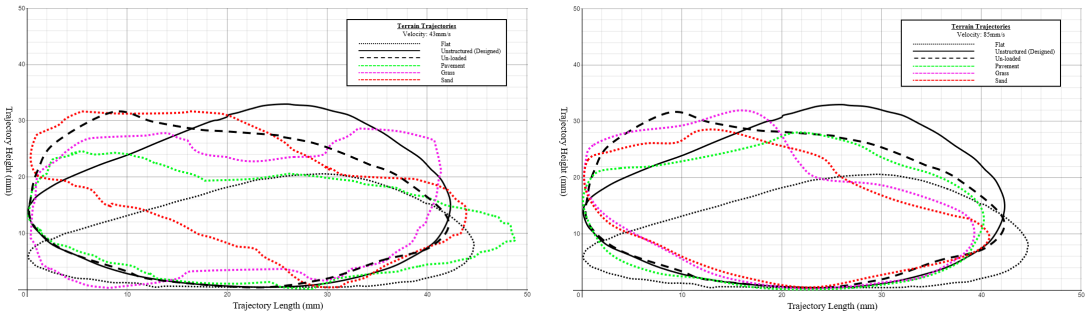

Fig. 14. Walking foot trajectories on different terrains at 43 mm/s (left) and 85 mm/s (right), incorporating the ”flat” walking trajectory from Figure 2 and the desired ”unstructured terrain” trajectory from Figure 4.

SUMMARY

This paper presents the robust design of a walking rover platform with six legs, each of which is an eight-bar linkage which design is based on a kinematic task that consists of nominal higher order specifications defined in the vicinity of two foot-environments contact locations. The design approach builds up incrementally starting with obtaining basic human leg walking trajectory, defining a ”relaxed” kinematic task with higher order constraints that are expressive enough to capture the system’s behavior in the vicinity of the foot-environments contacts, and creating a leg image through exploration of morphological and material properties. Finally, a six-legged robot platform prototype is assembled and tested. The pilot experimental results suggest that the proposed ”relaxed” kinematic task combined with the leg morphological properties and materials allowed the platform to walk stably on three different terrains. The ”relaxed” task introduced flexibility to the shape of the foot trajectory, while the specific leg morphology took care of the distribution of the forces throughout the rover body as it interacted with the terrains and made it adaptive. The slightly rubbery feet provided an additional degree of freedom for self-stabilization. Future work relates to the detailed testing and performance evaluation of the final prototype, as well as the investigation of the ability of the platform to generalize to other terrains.

ACKNOWLEDGEMENTS

The authors acknowledge the support of NSF CAREER Award ID 1751770, as well as the assistance of California State University, Fullerton students Aaron Fernandez and Kyle Skulski.

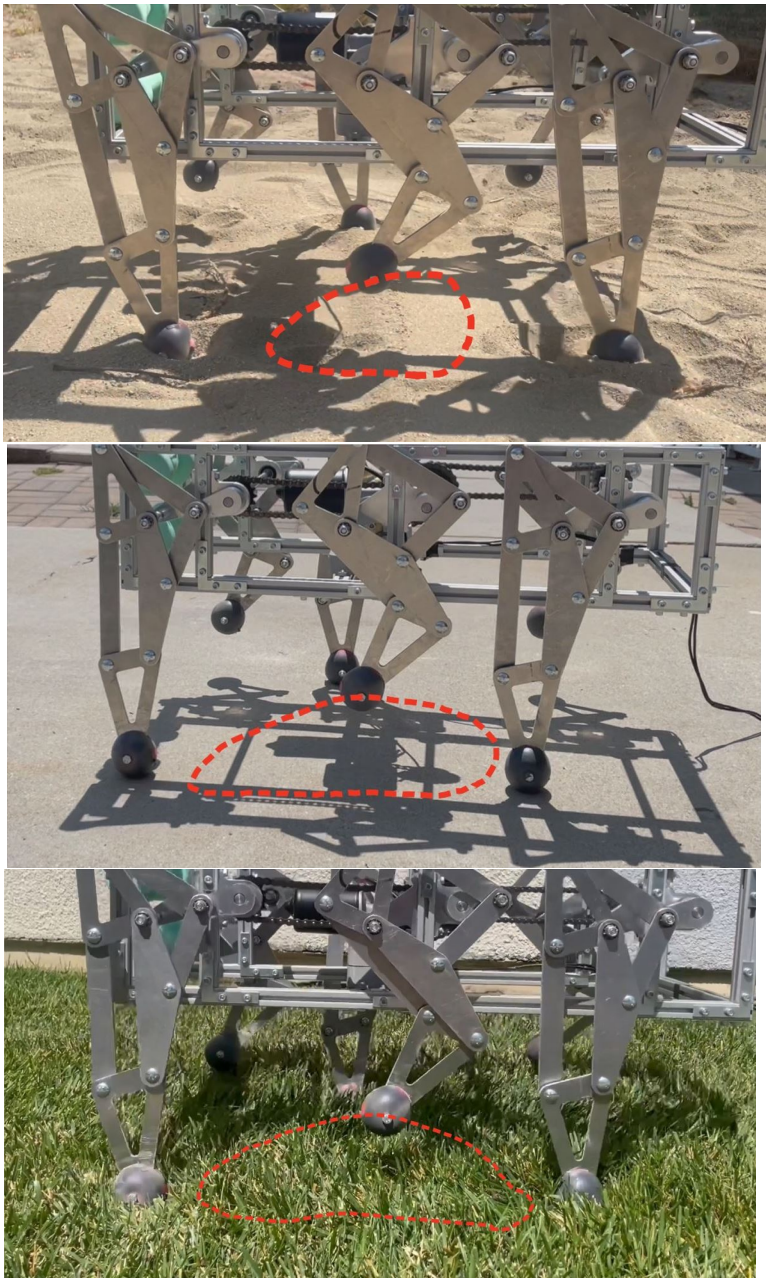

Fig. 15. Testing of the final prototype traversing sand (top), pavement (middle), and grass (bottom) terrains with a baseline velocity. The walking trajectories are based on tracking the middle point of the middle foot of the rover platform.

REFERENCES

[1] CSIRO, 2018, ICRA2018 Workshop: Multilegged Robots – Towards Robust Real-World Deployments URL research.csiro.au/robotics/multilegged-robots-workshop-icra2018/.

[2] Hoggett, R., 1983, ODEX-1 Functionoid Walking Robot 1983 URL https://youtube.com/watch?v=EWX9iRw33OE.

[3] Hoggett, R., 2010, OSU Adaptive Suspension Vehicle URL https://youtube.com/watch?v=DIiD1JimBXQ.

[4] MIT, 2010, MIT Cheetah Robot Lands the Running Jump URL https://youtube.com/watch?v=_luhn7TLfWU.

[5] Robotics, and Group, A. S., 2017, MAX: Multilegged Autonomous eXplorer URL https://research.csiro.au/robotics/max/.

[6] Robotic Systems Lab: Legged Robotics at ETH Zürich, 2017, ANYmal URL https://rsl.ethz.ch/robots-media/anymal.html.

[7] Dynamics, B., 2019, Spot Boston Dynamics URL https://www.bostondynamics.com/products/spot.

[8] NASA-JPL, 2013, Robosimian URL https://www.jpl.nasa.gov/robotics-at-jpl/robosimian.

[9] Karlsruhe, F. F. I., 1994, Lauron v URL https://en.wikipedia.org/wiki/LAURON.

[10] Moore, E., Campbell, D., Grimminger, F., and Buehler, M., 2002, "Reliable stair climbing in the simple hexapod 'rhex'," In Proceedings 2002 IEEE International Conference on Robotics and Automation (Cat. No.02CH37292), Vol. 3, pp. 2222–2227 vol.3.

[11] Saranli, U., Buehler, M., and Koditschek, D., 2001, "Rhex: A simple and highly mobile hexapod robot," *Departmental Papers (ESE),* **20**, 07.

[12] Pfeifer, R., and Bongard, J., 1984, *How the Body Shapes the Way We Think: A New View of Intelligence*, Vol. 1 Princeton University Press.

[13] Kamimura A, Kurokawa H, Y. E. e. a., 2005, "Automatic Locomotion Design And Experiments For A Modular Robotic System," In IEEE ASME Trans Mechatron, IEEE, pp. 314–325.

[14] Sun, Y., Ma, S., Yang, Y., and Pu, H., 2013, "Towards Stable and Efficient Legged Race-Walking of an ePaddle-Based Robot," *Mechatronics,* **23**(1), pp. 108–120.

[15] Paul, C., Roberts, J., Lipson, H., and Valero Cuevas, F., 2005, "Gait Production In A Tensegrity Based Robot," In ICAR '05. Proceedings., 12th International Conference on Advanced Robotics, 2005., pp. 216–222.

[16] Hutter, M., Remy, C. D., Hoepflinger, M. A., and Siegwart, R., 2013, "Efficient And Versatile Locomotion With Highly Compliant Legs," *IEEE/ASME Transactions on Mechatronics,* **18**(2), pp. 449–458.

[17] Paul, C., 2006, "Morphological Computation: A Basis For The Analysis Of Morphology And Control Requirements," *Robotics Auton. Syst.,* **54**, pp. 619–630.

[18] Tsujita, K., Kobayashi, T., Inoura, T., and Masuda, T., 2008, "Gait Transition by Tuning Muscle Tones using Pneumatic Actuators in Quadruped Locomotion," pp. 2453 – 2458.

[19] Cham, J. G., Karpick, J. K., and Cutkosky, M. R., 2004, "Stride Period Adaptation of a Biomimetic Running Hexapod," *The International Journal of Robotics Research,* **23**(2), pp. 141–153.

[20] Fukuoka, Y., Kimura, H., and Cohen, A. H., 2003, "Adaptive Dynamic Walking of a Quadruped Robot on Irregular Terrain Based on Biological Concepts," *The International Journal of Robotics Research,* **22**(3-4), pp. 187–202.

[21] Nansai, S., Rojas, N., Mohan, R. E., Sosa, R., and Iwase, M., 2015, "On A Jansen Leg With Multiple Gait Patterns For Reconfigurable Walking Platforms," *Advances in Mechanical Engineering,* **7**, 03.

[22] BBC, 2010, Theo Jansen's Strandbeests - Wallace Gromit's World of Invention - BBC One URL

`https://www.youtube.com/watch?v=HSKyHmjyrkA`.

[23] Robson, N. P., and McCarthy, J. M., 2007, "Kinematic Synthesis With Contact Direction And Curvature Constraints On The Workpiece," In ASME 2007 International Design Engineering

Technical Conferences and Computers and Information in Engineering Conference, American Society of Mechanical Engineers, pp. 581–588.

[24] Robson, N., and Ghosh, S., 2015, "Geometric Design of Planar Mechanisms Based on Virtual Guides for Manipulation," *Robotica,* **1**, 03, pp. 1–16.

[25] Moon, H., Baumgartner, H., and Robson, N. P., 2011, "Toward a 21st Century Crutch Design for Assisting Natural Gait,".

[26] Ghosh, S., Robson, N., and McCarthy, J., 2020, "Kinematic design and evaluation of a six-bar knee-ankle-foot orthosis," *Journal of Engineering and Science in Medical Diagnostics and Therapy,* **3**, 02.

[27] Robson, N. P., Ghosh, S., and Soh, G. S., 2019, "Kinematic synthesis and design of the robust closed loop articulated minimally actuated (clam) hand," *Robotica,* **38**, pp. 1921 – 1939.

[28] Robson, N., and Soh, G. S., 2016, "Geometric design of eight-bar wearable devices based on limb physiological contact task," *Mechanism and Machine Theory,* **100**, pp. 358–367.

[29] Zhang, L.-x., Wang, L.-j., Wang, F.-l., and Wang, K.-k., 2009, "Gait simulation of new robot for human walking on sand," *Journal of Central South University of Technology (English Edition),* **16**, 12, pp. 971–975.

[30] Ghosh, S., Robson, N., and McCarthy, J., 2015, "Geometric design of a passive mechanical knee for lower extremity wearable devices based on anthropomorphic foot task geometry scaling,".

[31] Craig, J. J., 2005, *Introduction to Robotics: Mechanics and Control*, Vol. 3 Pearson Prentice Hall Upper Saddle River.

[32] McCarthy, J., 2019, *Kinematic Synthesis of Mechanisms: A Project Based Approach* McCarthy Design Associates Publishing.

[33] SimiSystems, 2009, Dog Gait Analysis in 3D with Simi Motion URL www.youtube.com/watch?v=5jbCFLR2oIQ&ab_channel=SimiSystems.

[34] Lee, T.-T., Liao, C.-M., and Chen, T., 1988, "On the stability properties of hexapod tripod gait," *IEEE Journal on Robotics and Automation,* **4**(4), pp. 427–434.

APPENDIX A: TABLE CAPTION LIST

Table 1. Task data for the synthesis of a planar RR chain based on the ”relaxed” scaled down motion task

Table 2. Link lengths of the resulting eight-bar linkage

APPENDIX B: FIGURE CAPTION LIST

Fig 1. A body with attached frame M moves in the vicinity of specified location and is in contact with two objects such that the trajectories of $\mathbf{A}$ and $\mathbf{B}$ have the radii of curvature, R_A and R_B, respectively. Note that the geometry setup is related to one contact location (either toe-off or heel-strike).

Fig 2. Natural walking gait cycle trajectories at foot and knee level, obtained from the Motion Capture System. Data for the additional three foot trajectories observable from walking on sand are adopted from [29] and incorporated to the ”flat” teardrop foot trajectory.

Fig 3. The obtained four-bar linkage with a coupler trajectory based on the scaled down ”relaxed” kinematic task consisting of two contact locations with higher order motion constraints.The base pivots are denoted by G1 and G2, while the moving pivots are W1 and W2. The coupler points **A** and **B** were already presented in Figure 1. Note that for this specific scaled down task, points **A** and **B** are at the knee level.

Fig 4. The created eight-bar leg linkage with the resulting foot trajectory, based on the ”relaxed” kinematic task. The eight-bar leg incorporates two four-bar linkages: the synthesized $G1G2W1W2$, as well as $G1G2W1W3$ that share the base frame and the driving link. A pantograph mechanism completes the design of the eight-bar leg by relocating and scaling up the resulting trajectory.

Fig 5. Link lengths of the leg mechanism.

Fig 6. CAD drawing of the rover platform that incorporates six legs, each of which is an eight-bar linkage.

Fig 7. In order to maximize surface area when traversing on deformable surfaces such as sand or grass, a spherical foot cap was designed. The foot cap size is based on the results in Figure 3. By scaling up results related to the locations of point A and B in Figure 3, the foot cap size/geometry has been determined.

Fig 8. 3D printed prototype of the walking rover and the resulting leg trajectory, while the platform is suspended in the air.

Fig 9. Rover Design Breakdown (Front Isometric View).

Fig 10. Pilot testing of the preliminary prototype traversing sand (top), pavement (middle), and grass (bottom) terrains with two different velocities: 43 mm/s (left) and 85 mm/s (right). The walking trajectories are based on tracking the middle point of the middle foot of the rover platform.

Fig 11. Pavement gait patterns with velocities of 43 mm/s and 85 mm/s respectively. Note that due to the synchronized foot motion on both sides of the rover, only the gait pattern on the right-hand side is shown.

Fig 12. Sand gait patterns with velocities of 43 mm/s and 85 mm/s respectively. Note that due to the synchronized foot motion on both sides of the rover, only the gait pattern on the right-hand side is shown.

Fig 13. Grass gait patterns with velocities of 43 mm/s and 85 mm/s respectively. Note that due to the synchronized foot motion on both sides of the rover, only the gait pattern on the right-hand side is shown.

Fig 14. Walking foot trajectories on different terrains at 43 mm/s (left) and 85 mm/s (right), incorporating the ”flat” walking trajectory from Figure 2 and the desired ”unstructured terrain” trajectory from Figure 4.

Fig 15. Testing of the final prototype traversing sand (top), pavement (middle), and grass (bottom) terrains with a baseline velocity. The walking trajectories are based on tracking the middle point of the middle foot of the rover platform.